Machinability analysis and optimisation of EDM in AA6082/ 3 wt. % BN/1wt. % MoS2 hybrid composites using entropy method weights integrated with Complex Proportional Assessment (COPRAS) method

karthik pandiyan G
Jafrey Daniel James D
Vinothkumar Sivalingam (svkceg@gmail.com)
Shandong University https://orcid.org/0000-0002-6705-5933
Arjun D
Gowtham S
Gokul Kannan P
Bhuvaneshwar K
Ramkumar R
Mohanraj Chandran

Research Article

Keywords: Hybrid composites, Machinability, EDM, Process parameters, Entropy weight, COPRAS

Posted Date: June 7th, 2022

DOI: https://doi.org/10.21203/rs.3.rs-1652154/v1

Abstract

An investigation was made on composites containing AA6082 as matrix and boron nitride/molybdenum disulphide (BN/MoS_2) used as reinforcement, which was 3 wt. % of BN and 1% MoS_2 hybrid composite materials were fabricated by stir casting methodology. Using electrical discharge machining (EDM) equipment, machinability studies were examined to achieve an optimal condition of process parameters. Taguchi (L27 orthogonal array) based design of experiments was employed for experiments to examine the influence of process parameters like pulse on time (Ton), peak current (IP) and gap voltage (V) on material removal rate (MRR), circularity (CIRC), electrode wear rate (EWR), and cylindricity (CYLD) were investigated. Multi Criteria Decision Making (MCDM) methodology was employed for the process parameters while machining AA6082/ 3 wt. % BN/1% MoS_2 hybrid composites. An entropy-based objective weights method was integrated with the complex proportional assessment (COPRAS) approach to assess the most excellent optimal level of process parameters. The entropy (W_j) weights were 0.1285, 0.1002, 0.5707 and 0.2005 for MRR, EWR, CIRC, and CYLD. The optimal conditions are obtained from the COPRAS method of relative significance score, and quantitative utility assessment score in the nineteenth experiment having the 15 A, 50 µs and 30 V with the relative significance score of 0.0735 with a higher quantitative utility score of 100% is achieved. Using an SEM, the machined surface is analysed for the micro-structural examination. At higher peak current (IP), micro-voids and craters with poor surface finish were achieved.

1. Introduction

Aluminium alloy (AA6082) is a medium-strength, lightweight alloy with excellent corrosion resistance in aerospace structural parts and marine applications [1]. Considering modern engineering disciplines, metal matrix composites incorporate two or more reinforcements that can meet the needs of a viable alternative to traditional materials [2]. The most frequent machining procedure for hard materials is electrical discharge machining (EDM). A spark is created between the electrode and the workpiece to remove the material. Any hard material may be machined until it becomes electrically conductive. Ceramic composites containing boron nitride (BN) and molybdenum disulphide (Mos_2) are employed in various high-temperature applications. Due to its intrinsic properties like hardness, high stiffness, low density, electrical conductivity, and very high strength, used in aircraft engines, level sensors, wear-resistant components, industrial wear, plastic forming, and complex moulds for metal and heat exchangers applications [3]. An electro-thermal approach is electrical discharge machining (EDM). In a dielectric medium, a direct current pulse generator generates high-frequency electric sparks between an electrode and a workpiece. The melted and evaporated workpiece surface develops a final shape that adheres to the electrode geometry. Kumar et al. [4] conducted the machinability analysis on AISI 420 stainless steel alloy using die-sinking EDM. Taguchi based grey relational analysis (T-GRA) used multi-variable optimisation to find the best optimal process parameters. The process parameters considered were gap voltage (V), pulse on time (T_{on}), and Pulse current (A); output characteristics were material removal rate (MRR) and electrode wear rate (EWR). The results show that pulse current was influenced by 63.71%, gap voltage by 13.26%, Ton by 10.88% and improvement in grey relational grade by 0.086.

In another study, Mukherjee et al. [5] investigated the machining studies on titanium foam by EDM under chamfered and hollow electrodes. In comparison to other process factors, the results show that current is the most important factor in electrode wear rate. Chamfered electrodes produce a hole with an oversize of 0.43%, with maximum MRR achieved using a hollow electrode. Tao Le [6] examined the powder mixed EDM (PMEDM) processes of SKD61 steel. By modifying process parameters such as Ton, peak current, and powder concentration, tungsten carbide powder mixed concentration was employed as a dielectric medium to achieve MRR and tool wear rate. Peak current, Ton, and powder concentration have been shown to effect surface integrity, with the MRR increasing by 63.36%.

Machinability performances were investigated on titanium alloy by using WEDM. The optimisation of process parameters was optimised by using a neural network. This proposed methodology helps to minimise machining time by increasing production and process efficiency [7]. Karthikeyan et al. [8] conducted the WEDM experiment on nickel-base superalloy (MONEL K-500). The process variables considered were Wire Tension (WT), Wire Feed Rate (WFR), Gap Voltage (GV), pulse off time (Toff), and Ton, varied by five levels. The Taguchi L25 orthogonal array is used to assess output characteristics such as Surface Roughness (Ra), Material Removal Rate (MRR), and Kerf Width (k), and machining reaction variables are optimised using the T-GRA technique. Zhang et al. [9] performed the ultra-sonic assisted and powdered mixed EDM experiment on the 7Cr13Mo steel. The results show that 78% of microhardness was increased, and 57% of MRR was enhanced. In another study, By using a powder metallurgy electrode, Sarmah et al. [10] was able to successfully modify the surface of Al-7075 alloy. When compared to the substrate material, the deposited layer has 1.5–2.5 times the micro-hardness. The machinability of Inconel 718 alloy underwire cut EDM and die-sinking EDM is investigated by Li et al [11]. The results demonstrate that copper coated SiC electrodes with greater MRR, EWR, and surface morphology were employed as electrodes (i.e. roughness and topography). In terms of EWR, surface roughness, and MRR, the manufactured Cu-Sic electrode performs better.

The machinability of EDM was investigated utilising an environmentally friendly form of EDM, namely (near dry and wet) circumstances. Pulsed off time and Ton were the process parameters that were examined. Two-phase dielectric mediums (air and EDM oil) are employed in near-dry circumstances, whereas EDM oil is used in wet settings. The approach of gas chromatography and mass spectrometry is used to analyse gas emissions. The results show that the parameters were optimised to achieve higher MRR with a reduction in gaseous emission of about 97%.[12]. Singh Bains et al. [13] performed the magnetic field-assisted EDM on SiC reinforced aluminium composite materials. To accomplish the output performance characteristics of MRR and Surface roughness, the input process parameters of Toff, Ton, peak current and magnetic field intensity, sic percentage of distribution, and tool electrode material were analysed. Magnetic field-assisted EDM produced increased surface quality and MRR, according to the findings. In the drilling process, machining experiments on nickel-titanium shape memory alloys were explored. The process parameters were optimised to achieve micromoles with reduction in machining time of about 50–65% compared to the standard EDM process[14]. Karthik Pandiyan et al. [15] investigate the machinability studies on Al/Sic composites using RSM. The process parameters selected in this study were peak current, Toff and Ton; on output characteristics evaluated were surface roughness and MRR. The desirability function analysis methodology was employed to predict the optimum level of parameters to achieve higher MRR with lowered surface roughness.

Similar work was also carried out by Karthik Pandiyan et al. [16] using Al/ SiC composites by using EDM. The current, peak current and gap voltage parameters were considered to achieve MRR, TWR and Circularity and cylindricity utilising the MCDM Codas method.

Mechanical and tribological properties were evaluated on the AA6061-T6/ Sic composites. The results show that the addition of reinforcements enhanced composite materials' mechanical and tribological properties.[17][18]. The tribological and Mechanical characteristics of Zro2/Al2014 composite materials were fabricated using stir casting methodology. The results show that the addition of reinforcements enhances the properties of composite materials. [19].Abrasive wear studies were carried out on polypropylene/cloisite 30B/ elvaloy AC3427 nanocomposite fabricated using the melt intercalation method. Tribological studies were employed by using a two-body abrasive wear methodology.[20].Optimisation of process parameters was carried out during the EDM machining for biomedical devices for their biocompatibility to enhance the high standard necessities for biomedical materials and their applications in implant manufacturing.[21].Machining studies were carried out by tungsten carbide (WC) coated electrode material on Ti-6Al-V alloy. The process parameters considered were frequency and width, voltage and current to achieve output characteristics on MRR and TWR and overcuts were examined. The process parameters were optimised by using GRA and ANOVA methodology [22].

Machinability studies on AISI-D3 steel were examined by using EDM. The process parameters influence the machinability nature of the materials by tool rotation on surface integrity, TWR and MRR. The results show that tool rotation influences about 49% enhancement in MRR and surface roughness enhancement of about 10%.[23].Optimisation studies were carried out on EDM machining of Monel 400 alloy by copper titanium diboride electrode material. The tiB2%, Ton, current, and flushing pressure achieve output characteristics like MRR and TWR [24]. Traditional electrode and cryogenic cooled electrode materials employed machinability examination on Al/10% SiC composites. The results show that cryogenic cooled electrode material reduces the electrode wear rate by 18%.[25].Machinability examinations on AISI-D2 steel by the CCEDM process reduced wear rate by about 20% and surface roughness by about 18% [26]. Machinability and optimisation studies were carried out on OHNS steel to achieve higher MRR with lowered surface roughness and machining time employing optimum process parameters. The best process parameters were determined using GRA and ANOVA methods [27]. Stanojkovic and Radovanovic [28] successfully used the COPRAS technique in a high-pressure coolant drilling procedure on Al alloy with a carbide tool. Varatharajulu et al. [29] performed a drilling experiment on magnesium AZ1 alloy and optimised the desirability function technique using TOPSIS and COPRAS top rankings. With a spindle speed of 4540 rpm and a feed rate of 0.076 mm/rev, the best combination was discovered using TOPSIS and COPRAS for simultaneous minimisation of all answers. For supplier selection, Ghorabaee et al. [30] examined the COPRAS approach in interval type-2 fuzzy sets. Mishra et al. [31] investigated the COPRAS technique for assessing the bioenergy production process's long-term viability. To analyse city compactness, Jurgis et al. [32] used the COPRAS technique. To choose effective dwelling house walls, Zavadskas and Kaklauskas [33] examined the COPRAS approach.

The literature reveals no such works related to fabrication and Machinability studies using electrical discharge machining of AA6082/ 3 wt. % BN/1% MoS2 hybrid composites. Most authors used traditional optimisation methodologies like GRA, Taguchi, and RSM techniques to investigate the parameters. Multi-criteria decision making methodology was not yet used to optimise the process parameters. MCDM approach based complex proportional assessment (COPRAS) approach was not used to optimise process parameters while machining the AA6082/ 3 wt. % BN/1% MoS2 hybrid composites. Parametric optimisation examinations were engaged in assessing the effect of process parameters like IP, Ton, and gap voltage on MRR, EWR, CIRC, and CYLD during the machining of composite materials. The current study investigates the multi-objective optimisation of process parameters by MCDM based COPRAS method. The best optimum process parameters were achieved from the COPRAS quantitative assessment scores. The results revealed higher MRR with lowered EWR, CIRC and CYLD as output performances were enhanced.

A flow chart for the current study involves the fabrication, machining and optimisation of entropy weights integrated with COPRAS methodology are represented in Fig. 1.

Figure 1 : Schematic layout of fabrication, machining, and optimisation of hybrid composites

2 Materials And Methods

2.1 Fabrication of composite materials

Stir casting is the most efficient way of producing composite materials. The AA6082 alloy was chosen as the matrix material, where the ceramic filler was selected as Boron Nitride (BN) and Molybdenum disulphide (MoS_2). The matrix alloy materials (alloy rod form) are procured from the Covai metal mart, Coimbatore, India. The commercially available BN (99.5% purity) and MoS_2 (99.9% purity) reinforcement powders were used as reinforcement procured from Parshwamani metals, Mumbai, India. The MoS_2 possesses excellent mechanical and tribological properties with high hardiness and density, which retain its properties even at elevated temperatures. Due to its high hardness nature, BN is chosen as filler material which enriches the mechanical properties. Due to its neutron absorbing ability, it is used in the reactor control rods and shielding instruments and reactor shutdown materials. MoS_2 acts as a solid lubricant that enriches the tribological properties and resists the material's wear rate. MoS_2 has high thermal conductivity and high thermal stability at high thermal shock resistance. The fabricated composite material was used as a reactor control rod appliance. Table 1 represents the properties (physical and chemical) of AA6082alloy.

Table 1
Represents the chemical composition and physical properties of AA6082alloy.

Chemical composition	
Elements in wt in %	Ti-0.01,Mg-1.08,V-0.01,Fe-0.17, Mn-0.52,cu-o.32,Si-0.63,Al-97.25
Physical properties	
Tensile strength MPa	140
Density (g/cm^3)	2.669
Hardness (HV)	65

Initially, the wrought AA6082 alloy was preheated and melted in the crucible furnace. To prevent oxidation, the reinforcement was preheated up to 800°C. When alloy gets melted, i.e. liquidus point, the addition of degasser removes the impurities from the molten metal alloy. Once the liquid state reached, the preheated reinforcement particles were supplied into the molten alloy. The following proper selection of process parameters was employed to fabricate the composite materials using the stir casting process were preheated temperature of matrix material at 850ºC, the preheated temperature of reinforcement (BN& MoS_2) at 800ºC for about 2 hours, the molten temperature of composite materials at 750ºC, Ultrasonic agitator having the 25KHz-frequency was used to blend the molten melt for 10 Min[17]. The ultrasonic agitation process of mixing the molten metal with the composite materials is the most effective methodology for fabricating composite materials with the homogeneous distribution of filler materials with the matrix materials. The proper bonding of matrix with the reinforcements was achieved by adding one wt. % magnesium into the molten metal. The molten composite materials were kept held at about 750°C. Once the agitation process was completed, the molten melt was allowed to feed into the preheated die. The die was preheated to 300ºC. After the solidification of molten metal, the fabricated composite materials were taken from the mould for the other machining process. Figure 2. shows the Schematic diagram for the fabrication of AA6082/BN/Mos2 composite materials

Figure 2 Schematic diagram for fabrication of AA6082 /3 Wt. % BN/1% MoS2 hybrid composite

2.2 Material characteristics

The material characterisation was employed once the composite materials were fabricated. As per ASTM standards, the fabricated composite materials were evaluated for mechanical characterisation. ASTM B557M, ASTME9-19M, ASTM E23, ASTM E10-08, and ASTM D792 standards were chosen to evaluate the Tensile, Compressive, Impact strength, Brinell hardness and Density measurement. Due to the Orowan strengthening mechanism, the tensile strength of the composite materials was enhanced, which is achieved by the homogeneous distribution of filler with the matrix materials. The proper bonding of reinforcement with the matrix materials leads to strength enhancement. Compressive strength enhancement was achieved by minor grain dislocation during the compression, which resists the dislocation of grains. The reinforcements resisted sudden impact loading, which absorbed the impact energy. During the solidification, Shrinkage porosity will occur, leading to differences in density. Mechanical characterisation reveals that the AA6082/ 3 wt. % BN/1% MoS2 hybrid composites reveal superior enriched properties.

2.3 Machining process

EDM Machinability examination was employed to fabricate the composite material once the fabrication process was over. The machinability of composite materials was tested using EDM (Die sinking type) equipment. Electrolyte industrial copper has used an electrode material (length-60mm, diameter-8 mm). A 100*100*10 mm composite material was used as a working specimen for machining, and the workpiece was held in the sink's machine vice. The workpiece acted as affirmative polarisation, and the copper electrode acted as pessimistic polarisation; supercut SE0501 oil was used as a dielectric medium, constant pressure of 15kg/cm^2. The 2 mm depth of cut was employed on the material for all sets of experiments. The geometric tolerances like CIRC and CYLD were measured by the Coordinate Measuring Machine (CMM). The output responses like MRR and EWR are evaluated by equations 1 &2. Table 2 represents the experimental details of EDM. Figure 3 shows the (a) Experimental setup and (b) Co-ordinate measuring machine.

Table 2
Experimental details of the EDM process

Workpiece material and electrode	AA6082-T6/3 wt% BN/1% MoS_2 composites (100*100*10mm) Copper (50 mm in length,8 mm in diameter)
Current (A)	9,12,15
Pulse on time(T_{on})	50,75,100
Gap voltage (V)	30,35,40
Dielectric fluid	EDM oil (supercut SE0501)
Polarity	Work piece (+ ve),Copper (-ve)
Servo feed	2100 units
Constant pressure	15kg/cm^2
Peak voltage	110 V DC

$$MRR = \left(\frac{W_{wb} - W_{wa}}{\rho} \right) \times M_t$$

1

$$EWR = \left(\frac{W_{eb} - W_{ea}}{\rho} \right) \times M_t$$

2

Where W_{wb}- weight before machining (workpiece); W_{wa}- weight after machining(workpiece); W_{eb}- weight before machining (Electrode); W_{ea}- weight after machining (Electrode); M_t- time taken for machining (min); ρ- work piece Density = 2.669 g/cm^3; ρ- Tool electrode Density = 8.96 g/cm^3

For experimentation, Taguchi (L27orthogonal array) based design of experiments was employed. The input process parameters chosen in this current examination were IP, T_{on}, and gap voltage and the output characteristics evaluated were MRR, EWR, CIRC and CYLD. Input parameter and output characteristics with weights are shown in Table 3.

Table 3
L27 orthogonal array experimental values

Sl.no	Weights criteria (W_j)			0.1285	0.1002	0.5707	0.2005
	Input Parameters			Output response			
	Current	Pulse on time	Gap voltage	MRR	EWR	CIR	CYL
	A	µs	V	g/min	g/min	mm	mm
1	9	50	30	0.1550	0.0198	0.0285	0.1724
2	9	50	35	0.2259	0.0264	0.0128	0.0572
3	9	50	40	0.1478	0.0148	0.0157	0.0446
4	9	75	30	0.2152	0.0264	0.0079	0.0528
5	9	75	35	0.2112	0.0211	0.0100	0.0460
6	9	75	40	0.1540	0.0183	0.0178	0.0428
7	9	100	30	0.2725	0.0284	0.0076	0.0478
8	9	100	35	0.2286	0.0248	0.0109	0.0428
9	9	100	40	0.1758	0.0176	0.0414	0.0373
10	12	50	30	0.2694	0.0269	0.0107	0.0513
11	12	50	35	0.3997	0.0400	0.0128	0.0436
12	12	50	40	0.3078	0.0294	0.0107	0.0392
13	12	75	30	0.3559	0.0412	0.0106	0.0724
14	12	75	35	0.4357	0.0261	0.0170	0.0444
15	12	75	40	0.3297	0.0285	0.0102	0.0353
16	12	100	30	0.4456	0.0466	0.0065	0.0422
17	12	100	35	0.4365	0.0437	0.0094	0.0370
18	12	100	40	0.2842	0.0284	0.0093	0.1315
19	15	50	30	0.3925	0.0393	0.0016	0.0405
20	15	50	35	0.6245	0.0574	0.0050	0.0449
21	15	50	40	0.4637	0.0445	0.0064	0.0595
22	15	75	30	0.5510	0.0463	0.0184	0.0343
23	15	75	35	0.5129	0.0513	0.0246	0.0516
24	15	75	40	0.3350	0.0273	0.0093	0.0308
25	15	100	30	0.4352	0.0435	0.0115	0.0472
26	15	100	35	0.5521	0.0473	0.0165	0.0258
27	15	100	40	0.4123	0.0323	0.0303	0.0561

Figure 3 show the (a) Experimental setup (b) Co-ordinate measuring machine.

3. Results And Discussion

3.1 Microstructure Examination

Figure 4 represents the optical microscopic images of casted AA6082/ 3 wt. % BN/1% MoS2 hybrid composites composite at etched condition. The images reveal that the bright zone represents the matrix material (AA6082 alloy) while the dark particles represent the reinforcement (BN&MoS2) presented on the composite materials. Etchant (Keller's reagent) was used for clear visible grains present on the surface of composites. The presence of fine grains of aluminium particles was observed due to the cooling rate of composite material during the solidification process during the casting. The presence of reinforcement (BN& MoS_2) with grain boundaries were found on the composite's surface. Predicated Mg_2Si particles were exhibited on the surface of the primary solid solution of aluminium matrix materials. The grain boundaries exhibited the trapped fine particles of reinforcements with dense distribution at a higher amount of reinforcements and uniform distribution over the surface.

Figure .4 shows the micrographs of a matrix of stir cast AA6082 /3 Wt. % BN/1% MoS2 hybrid composite at the etched condition

Figure 5 represents the SEM micrographs of stir cast AA6082/3 wt. % BN/MoS2 composite. From the macroscopic images, it is observed that AA6082 alloy with interfacial bonding with BN and MoS_2 particles. The fabricated specimen exhibits the uniform dispersion of ceramic reinforcement with less amount of porosity is evidenced.

Figure 5. **SEM image of AA6082/3 Wt. % BN/1% MoS_2 hybrid composite**

3.2 Effect of input parameters on output characteristics

3.2.1 Material Removal Rate (MRR)

Figure 6 represents a diagram to understand this process, where MRR increases with increasing IP with various gap voltage in the machining of hybrid composites. Authors conclude that evidence is strong with increases in IP results more spark energy being generated in the intermediated zone of the workpiece- electrode, thus enhancing the MRR. Ton increase with increases in MRR due to continuous plasma channel in the machine zone workpiece getting melt and vaporised, resulting in an enhancement in MRR which is done by increasing the gap voltage rose from low to medium, then declined at the higher level. The MRR declined where the gap voltage increased.[25]. At a higher level of gap voltage, the liberation of energy was more, resulting in a void on the surface and a lower MRR. When IP and Ton are combined, the enhancement of MRR is accomplished by enhancing the IP and Ton[34]. MRR amplified as IP was increased where V and IP were combined. MRR was enhanced by enhancing the gap voltage from a low to an intermediate level, followed by dropping at the higher level. MRR enhances Ton from a minimum to a maximum level when gap voltage & Ton are combined. MRR enhances by enhancing the gap voltage from minimum to intermediate level. A reduction of MRR occurred due to the maximum level of gap voltage when both were combined[35].MRR enhancement may occur by enhancing the IP from minimum to maximum level. The enhancement of gap voltage from minimum to intermediate level followed by reduction will occur at the maximum level when IP and gap voltage is combined.

Figure .6 the Impact of input parameters on MRR.

3.2.2 Electrode Wear Rate (EWR)

Electrode wear rate plays a significant role in EDM machining because the shape of the electrode is reproduced in the workpiece surface. More amount of EWR affects the workpiece geometry. At the same time, it was increasing the IP, a sudden rise in EWR. More dissipation energy was produced during the process, resulting in a greater EWR[36]. EWR reduced as Ton increased from a minimum to an intermediate level and grew as Ton amplified. The higher IP and Ton result in higher plasma energy generated near the vicinity of electrode and workpiece due to this workpiece surface layer melting and evaporating. This resulted in an EWR increase up to an intermediate level, then a diminished at a maximum level. EWR is enhanced when voltage grows from a minimum to an intermediate level, and then the reduction will occur at the maximum level. Gap voltage enhances with a diminished MRR, resulting in considerable discharge energy. As a result, voids formed on the surface, and EWR was lowered. EWR increased when IP increased from a minimum to a higher level when combined IP and Ton. EWR grew from a low to an intermediate level, then reduced as Ton increased[25]. When gap voltage and IP were combined, EWR enhanced the IP. EWR improved as voltage grew from a minimum to an intermediate level; it then fell when voltage increased to a maximum level due to persistent sparking. EWR enhances the voltage from a minimum to an intermediate level and then diminishes with amplifying the voltage from a minimum to an intermediate level and then declines at the maximum level when both Ton and gap voltage are combined. Electrode Wear rate improved with enhancement in Ton from a minimum to an intermediate level and declined at a maximum level when gap voltage and IP were combined. EWR improved as voltage grew from a minimum to an intermediate level, and then diminished as voltage amplified to a maximum level. The impact of process parameters on EWR is representing in Fig. 7.

Figure 7 **the Impact of input parameters on EWR.**

3.2.3 Circularity (CIRC)

CIRC decreases as IP rises from a low to an intermediate level, then rises again at a maximum level. The CIRC increased due to more energy liberation during the machining process. With an increase in Ton, CIRC rose. A higher Ton created a greater quantity of discharge energy, allowing the workpiece material to evaporate and melt. As a result, CIRC increased. CIRC rises as the gap voltage rises from minimum to maximum levels[37]. CIRC enhanced the IP and Ton when both IP and Ton were combined. CIRC enhances the IP from a minimum to an intermediate level when both IP and voltage are combined and reduces with an increase in voltage and IP when both are combined. As the gap voltage was increased from a low to a higher level, CIRC decreased. [38]. CIRC is enhanced with a rising the Ton from a minimum to an intermediate level and then reduced with an enhancing the Ton. When both gap voltage and Ton were combined, CIRC was extended by amplifying the voltage from a low to an intermediate level and then reduced at the highest level. When both IP and gap voltage are combined, CIRC rises with a rise in Ton and voltage from a low to an intermediate level and falls at a high level.[37, 38]. The effect of process parameters on CIRC is represented in Fig. 8.

Figure 8. **The Impact of input parameters on CIR.**

3.2.4 Cylindricity (CYLD)

From a minimum to an intermediate level, CYLD grew with a rise in IP and Ton and then diminished at a maximum level. More discharge energy was created during the process, resulting in a greater CYLD. The energy released at a greater Ton higher liberation of energy legitimate the material to evaporate and melt. This resulted in a rise in CYLD. When the gap voltage was enhanced from a minimum to a maximum level, CYLD increased. By combining Ton and IP, CYLD enlarged when IP and Ton amplified from a minimum to an intermediate level, then declined as IP and Ton increased to a high level. When IP and voltage were coupled, CYLD became larger with an increase in IP and voltage from a low to a medium level, and shrank with an increase in IP and voltage from a high to a low level. CYLD was improved when the gap voltage was increased from a minimum to a maximum level [39]. When Ton and voltage were mixed, CYLD

enhanced by amplifying them from a low to a medium level and decreased by raising them to a maximum level. CYLD grew when the gap voltage was increased from a low to a high level. CYLD improved as the IP and voltage were amplified from a low to a medium level, then diminished when the gap voltage and IP were combined [40]. The impact of process parameters on CYLD is representing in Fig. 9.

Figure 9. **the Impact of input parameters on CYLD.**

3.3 Weightage entropy method

Entropy is the most efficient objective weighting method used to evaluate the weights of the MCDM problems[16]. This method employs positioning the alternative with their performance characteristics to determine the optimal process parameters. Entropy integrated COPRAS method as follows

Entropy methodology:

Stage 1: Normalisation of the assessment matrix (P_{ij})

$$P_{ij} = \frac{x_{ij}}{? \sum_{i=1}^{m} x_{ij}}$$

3

$(i ? \{1,2, \ldots n\}, (j ? \{1,2, \ldots m\});$ X_{ij} - i^{th} characteristics on j^{th} decisive factor performance.

Stage 2: determination of entropy measure

$$E_j = -K ? \sum_{i=1}^{m} p_{ij} ln p_{ij}$$

4

Where$k = 1/\ln(m)$.

Stage 3: Estimation of entropy

$$W_j = \frac{1 - E_j}{? \sum_{j=1}^{n} (1 - E_{j)}}$$

5

W_j - weight criterion

3.4Optimization by COPRAS

Zavadskas developed the COPRAS methodology in 1994. This method assumes proportionality to the consequence and utility degree of alternatives at variance criteria and considers both the ultimate most excellent and the ultimate most horrible solution. It is a compensatory method where the attributes are independent. The following expressions were defined by the COPRAS method.

Stage1 Construction of initial decision matrix (X)

$$X - \left[x_{ij}\right]_{nXm} = \begin{bmatrix} x_{11} & x_{12} & \cdots & x_{1n} \\ x_{21} & x_{22} & \cdots & x_{2n} \\ \vdots & \vdots & \vdots & \vdots \\ x_{m1} & x_{m2} & \cdots & x_{mn} \end{bmatrix}$$

6

Where n is the No. of criteria, m is the No. of alternatives.

Stage2 Estimation of normalised decision matrix.

R=[rij]=$\frac{x_{ij}}{il ? \sum_{i=1} ? x_{ij}}$ (7)

Step 3 Estimation of the weighted normalized matrix

$$D = \left[y_{ij} \right]_{mxn} = r_{ij} x w_j$$

8

$y_{ij}$is the weights criteria, lies in-between from 0 to 1. w_j -weight for j^{th} alternative. The summation of weights is equal to 1 i.e($? \sum_{j=1}^{m} w_j = 1$).i = 1,2,.....m and j = 1,2,.....n

Stage 4 Summation of normalized weighted decision matrix

$$S_{+i} = \sum_{j=1}^{n} ? y_{+ij}$$

$$S_{-i} = \sum_{j=1}^{n} ? y_{-ij}$$

9

Where S_{+i}= sum of favourable characteristics, s_{-i}= sum of non favourable characteristics.

Stage 5 Determine relative significance of alternatives

$$Q_i = S_{+i} + \frac{S_{-min} \sum_{i=1}^{m} ? S_{-i}}{S_{-i} \sum_{i=1}^{m} ? \left(S_{-min} / S_{-i} \right)}$$

10

S_{-min}= S_{-i}, for (i = 1,2,.....m)

Stage 6 Determination of quantitative utility (U_i)

$$U_i = \left[\frac{Q_i}{Q_{max}} \right] \times 100\%$$

11

Step7 Ranking of quantitative utility (U_i) score. The highest Ui is the most excellent best possible score.

Table 4 represents the optimisation by the COPRAS method.

Table 4
Optimisation by Entropy weights incorporated with COPRAS

S.No	Normalised Decision Matrix				Weighted Normalised Decision Matrix				sum of beneficial S + i	s-i	s-min/s-i	Q_i	U_i
	MRR	EWR	CIRC	CYLD	MRR	EWR	CIRC	CYLD					
1	0.0166	0.0221	0.0763	0.1204	0.0021	0.0022	0.0436	0.0242	0.0021	0.0699	0.1788	0.0150	19.390
2	0.0242	0.0294	0.0343	0.0400	0.0031	0.0029	0.0196	0.0080	0.0031	0.0305	0.4096	0.0326	42.123
3	0.0158	0.0165	0.0420	0.0312	0.0020	0.0017	0.0240	0.0062	0.0020	0.0319	0.3920	0.0302	39.090
4	0.0231	0.0294	0.0212	0.0369	0.0030	0.0029	0.0121	0.0074	0.0030	0.0224	0.5576	0.0431	55.696
5	0.0226	0.0235	0.0268	0.0321	0.0029	0.0024	0.0153	0.0064	0.0029	0.0241	0.5190	0.0403	52.037
6	0.0165	0.0204	0.0477	0.0299	0.0021	0.0020	0.0272	0.0060	0.0021	0.0352	0.3547	0.0276	35.731
7	0.0292	0.0316	0.0204	0.0334	0.0038	0.0032	0.0116	0.0067	0.0038	0.0215	0.5820	0.0456	58.983
8	0.0245	0.0277	0.0292	0.0299	0.0031	0.0028	0.0167	0.0060	0.0031	0.0254	0.4916	0.0385	49.797
9	0.0188	0.0196	0.1109	0.0261	0.0024	0.0020	0.0633	0.0052	0.0024	0.0705	0.1774	0.0152	19.631
10	0.0289	0.0300	0.0287	0.0358	0.0037	0.0030	0.0164	0.0072	0.0037	0.0265	0.4709	0.0376	48.596
11	0.0428	0.0445	0.0343	0.0305	0.0055	0.0045	0.0196	0.0061	0.0055	0.0301	0.4149	0.0354	45.704
12	0.0330	0.0328	0.0287	0.0274	0.0042	0.0033	0.0164	0.0055	0.0042	0.0251	0.4974	0.0400	51.747
13	0.0382	0.0459	0.0284	0.0506	0.0049	0.0046	0.0162	0.0101	0.0049	0.0309	0.4040	0.0340	43.913
14	0.0467	0.0291	0.0455	0.0310	0.0060	0.0029	0.0260	0.0062	0.0060	0.0351	0.3560	0.0316	40.865
15	0.0353	0.0317	0.0273	0.0247	0.0045	0.0032	0.0156	0.0049	0.0045	0.0237	0.5272	0.0425	54.905
16	0.0478	0.0519	0.0174	0.0295	0.0061	0.0052	0.0099	0.0059	0.0061	0.0210	0.5940	0.0489	63.180
17	0.0468	0.0486	0.0252	0.0259	0.0060	0.0049	0.0144	0.0052	0.0060	0.0244	0.5119	0.0428	55.381
18	0.0305	0.0317	0.0250	0.0919	0.0039	0.0032	0.0142	0.0184	0.0039	0.0358	0.3488	0.0290	37.504
19	0.0421	0.0437	0.0043	0.0283	0.0054	0.0044	0.0024	0.0057	0.0054	0.0125	1.0000	0.0774	100.00
20	0.0669	0.0640	0.0134	0.0314	0.0086	0.0064	0.0076	0.0063	0.0086	0.0203	0.6144	0.0528	68.268
21	0.0497	0.0496	0.0171	0.0416	0.0064	0.0050	0.0098	0.0083	0.0064	0.0231	0.5415	0.0453	58.621
22	0.0591	0.0516	0.0493	0.0240	0.0076	0.0052	0.0281	0.0048	0.0076	0.0381	0.3282	0.0312	40.333
23	0.0550	0.0571	0.0659	0.0361	0.0071	0.0057	0.0376	0.0072	0.0071	0.0506	0.2473	0.0249	32.133
24	0.0359	0.0304	0.0249	0.0215	0.0046	0.0030	0.0142	0.0043	0.0046	0.0216	0.5794	0.0463	59.857
25	0.0466	0.0485	0.0308	0.0330	0.0060	0.0049	0.0176	0.0066	0.0060	0.0290	0.4304	0.0370	47.779
26	0.0592	0.0527	0.0442	0.0180	0.0076	0.0053	0.0252	0.0036	0.0076	0.0341	0.3664	0.0340	43.913
27	0.0442	0.0359	0.0811	0.0392	0.0057	0.0036	0.0463	0.0079	0.0057	0.0578	0.2164	0.0212	27.468
									s-min	0.012503			

Eqn 3–5 are used to calculate the entropy weightage for individual output responses such as MRR, TWR, CIR and CYL are 0.1285, 0.1002, 0.5707 and 0.2005, respectively. The normalised decision matrix is computed by Eq. 6–7. Obtained weightage values are multiplied with the normalised matrix; the weightage normalised decision matrix is calculated by Eq. 8. Eq. 9 are used to calculate the summation of the normalised decision matrix for beneficial and non-beneficial chrematistics for MRR, EWR, CIRC and CYLD. The relative significance of alternatives is computed by Eq. 10. From the set of all experiments, Eq. 11 is used to calculate the best optimum set achieved by the higher quantitative utility (Ui) score, which was considered the best optimum level of experiments. From the results, it is observed that the experiment number nineteen showed higher COPRAS- quantitative utility (Ui) score of 100% with a relative significance score of 0.0735, which was considered the best optimal parameter achieved at 3 wt % of BN, 15 A, 50 µs and 30 V exhibits enhanced yield performance characteristics.

According to the quantitative utility score obtained from the COPRAS method, the alternatives values were ranked as follows

26 < 18 < 21 < 9 < 10 < 22 < 5 < 12 < 25 < 13 < 15 < 11 < 17 < 19 < 7 < 3 < 8 < 27 < 1 < 2 < 6 < 20 < 23 < 4 < 14 < 16 < 24.

3.5 Micro-structural analysis at the Optimum parameter

The micro-structural examination was employed on the machined surface examined via SEM. Figure 10(a) the Machined surface of AA6082/3 Wt.% BN/1% MoS_2 composite at a higher level process parameters of (IP) = 15A; (T_{on}) = 100 µs; V = 40 V. 10 (b) the Machined surface of AA6082/3 Wt.% BN/1% MoS_2 composite at optimum level of (IP) = 15A; (T_{on}) = 50 µs; V = 30 From the Fig. 10(a), it is observed that at elevated IP and T_{on} microvoids and craters were evident on the machined surface. At higher IP with T_{on}, the micro-cracks, craters, and voids were generated due to the liberation of an elevated amount of energy that breaks the reinforcement particles in the matrix materials. Figure 10 (b) shows that At optimum level process parameters, higher-level IP, with lowered the gap voltage and Ton, the liberation of energy generated during the process, which leads to increases in MRR and lowered the EWR achieved by the soft nature of matrix materials. Tool strike the reinforcement, which leads to enhancement of EWR. At higher level process parameters, the size of craters increased with an increase in T_{on}. The formation of voids is due to the high amount of plasma energy formed between the tool and workpiece. At the optimum level, Low gap voltage enhanced the surface finish. High gap voltage leads to poor surface finish.at the higher-level process parameters more microvoids were evident on the surface when compared to the optimum level process parameters Fig. 10(a) the Machined surface of AA6082/3 Wt.% BN/1% MoS_2 composite at a higher level process parameters of (IP) = 15A; (T_{on}) = 100 µs; V = 40 V. 9 (b) the Machined surface of AA6082/3 Wt.% BN/1% MoS_2 composite at optimum level of (IP) = 15A; (T_{on}) = 50 µs; V = 30 V.

Conclusions

AA6082/ 3 wt. % BN/1% MoS_2 hybrid composites were fabricated by stir casting methodology. EDM experiments were carried out on the fabricated hybrid composite materials to study the influences of machining parameters, i.e. current, pule on time and gap voltage and MRR, EWR, CYLD and CIRC. The complex proportional assessment (COPRAS) approach evaluates the optimum machining sets for the EDM process. The main findings were obtained from the experimental studies

1. From the COPRAS quantitative Assessment score, at IP = 15A; T_{on} = 50 µs; gap voltage = 30 V were attained, which is the best optimal parameter possesses enhancement of MRR and lowered the EWR, CIRC and CYLD.
2. The most excellent optimal factor was achieved in the 19th experimental run having a significance value of 0.0735. Entropy weights for MRR, EWR, CIRC, and CYLD are 0.1285, 0.1002, 0.5707 and 0.2005, respectively. MRR is enhanced by enhancing the IP and decreasing the T_{on}.
3. EWR is enhanced by enhancing the T_{on} and gap voltage. Increasing IP and $T_{on,}$ CIRC was enhanced.
4. CYLD declined by amplifying the IP and lowered T_{on}. By SEM, the machined surfaces were examined. Better surface finish with a minimum size of craters and micro-voids were found on the surface by increasing IP and lowering the T_{on} and gap voltage.

Declarations

Funding : This work is supported by Fundamental Research Funds of Shandong University [2019HW040]. Future for Young Scholars of Shandong University, China (31360082064026).

Availability of data and material : Not applicable

Code availability: Not applicable

Conflicts of interest :The authors declare no conflict of interest.

Ethics approval: Not applicable

Consent to participate: Not applicable

Consent for publication: Not applicable

Authors' contributions

Karthik Pandiyan G: Conceptualization, Experimental work & Data curation Writing – review & editing, Jafrey Daniel James D: Data curation Writing – review & editing, Vinothkumar Sivalingam: Data curation Writing – review & editing, Arjun D: Experimental work & Data curation, Gowtham S: Experimental work & Data curation, Gokul Kannan P: Experimental work & Data curation, Bhuvaneshwar K: Experimental work & Data curation, Ram Kumar R: Writing – review & editing Mohanraj Chandran: Writing – review & editing.

References

1. Sivanesh Prabhu M, Elaya Perumal A, Arulvel S, Franklin Issac R (2019) Friction and wear measurements of friction stir processed aluminium alloy 6082/CaCO3 composite. Measurement 142:10–20. https://doi.org/https://doi.org/10.1016/j.measurement.2019.04.061
2. Sharma P, Sharma S, Khanduja D (2015) A study on microstructure of aluminium matrix composites. J Asian Ceram Soc 3:240–244. https://doi.org/https://doi.org/10.1016/j.jascer.2015.04.001
3. Mohd Abbas N, Solomon DG, Fuad Bahari M (2007) A review on current research trends in electrical discharge machining (EDM). Int J Mach Tools Manuf 47:1214–1228. https://doi.org/https://doi.org/10.1016/j.ijmachtools.2006.08.026
4. Kumar S, Ghoshal SK, Arora PK, Nagdeve L (2021) Multi-variable optimization in die-sinking EDM process of AISI420 stainless steel. Mater Manuf Process 36:572–582. https://doi.org/10.1080/10426914.2020.1843678

5. Mukherjee S, Rai D, Giridharan A (2021) EDM of titanium foam: electrode wear rate, oversize, and MRR. Mater Manuf Process 1–13. https://doi.org/10.1080/10426914.2021.1981938
6. Tao Le V (2021) The influence of additive powder on machinability and surface integrity of SKD61 steel by EDM process. Mater Manuf Process 1–15. https://doi.org/10.1080/10426914.2021.1885710
7. Uma Maheshwera Reddy Suryapavan Cheruku, Salike S, Kumar Pasunuri VP NSR (2022) Estimation of machinability performance in wire-EDM on titanium alloy using neural networks. Mater Manuf Process 1–12. https://doi.org/10.1080/10426914.2022.2030875
8. Karthikeyan AG, Kalaiselvan K, Muralidharan N (2021) CNC wire-cut EDM input variables analysis on Ni -based superalloy (MONEL K-500). Mater Manuf Process 1–10. https://doi.org/10.1080/10426914.2021.2001522
9. Zhang W, Li L, Wang N, Teng YL (2021) Machining of 7Cr13Mo steel by US-PMEDM process. Mater Manuf Process 1–7. https://doi.org/10.1080/10426914.2021.1885704
10. Sarmah A, Kar S, Patowari PK, Sarmah A (2020) Surface modification of aluminum with green compact powder metallurgy Inconel-aluminum tool in EDM Surface modification of aluminum with green compact powder metallurgy Inconel-. Mater Manuf Process 00:1–9. https://doi.org/10.1080/10426914.2020.1765253
11. Li L, Li ZY, Wei XT, Cheng X (2015) Machining Characteristics of Inconel 718 by Sinking-EDM and Wire-EDM. Mater Manuf Process 30:968–973. https://doi.org/10.1080/10426914.2014.973579
12. Dhakar K, Chaudhary K, Dvivedi A, Bembalge O (2019) An environment-friendly and sustainable machining method: near-dry EDM. Mater Manuf Process 34:1307–1315. https://doi.org/10.1080/10426914.2019.1643471
13. Singh Bains P, Sidhu SS, Payal HS (2018) Investigation of magnetic field-assisted EDM of composites. Mater Manuf Process 33:670–675. https://doi.org/10.1080/10426914.2017.1364857
14. Al-Ahmari AMA, Rasheed MS, Mohammed MK, Saleh T (2016) A Hybrid Machining Process Combining Micro-EDM and Laser Beam Machining of Nickel–Titanium-Based Shape Memory Alloy. Mater Manuf Process 31:447–455. https://doi.org/10.1080/10426914.2015.1019102
15. Karthik pandiyan G, Prabaharan T, Jafrey Daniel James D, Vinothkumar sivalingam;Thangapandian N (2021) Improvement on the machinability characteristics of AA6061-T6 / 15 wt.% SiC composites by Response Surface methodology. Surf Topogr Metrol Prop 9:35050. https://doi.org/10.1088/2051-672X/ac2560
16. Pandiyan GK, Prabaharan T, James DJD, Sivalingam V (2021) Machinability Analysis and Optimization of Electrical Discharge Machining in AA6061-T6 / 15wt.% SiC Composite by the Multi-criteria Decision-Making Approach. J Mater Eng Perform. https://doi.org/10.1007/s11665-021-06511-8
17. Karthik Pandiyan G, Prabaharan T (2021) Mechanical and Tribological Characterization of Stir Cast AA6061 T6 – SiC Composite. Silicon 13:4575–4582. https://doi.org/10.1007/s12633-020-00781-y
18. Karthik Pandiyan G, Prabaharan T (2020) Optimization of machining parameters on AA6351 alloy steel using Response Surface Methodology (RSM). Mater Today Proc 1–4. https://doi.org/10.1016/j.matpr.2020.01.369
19. Ganesh Babu JDanielJD, Ramesh L, Ravichandran M MM (2019) Mechanical and tribological characteristics of ZrO2 reinforced Al2014 matrix composites produced via stir casting route. Mater Res Express 6:115542. https://doi.org/10.1088/2053-1591/ab4fc1
20. Daniel DJ, Panneerselvam K (2018) Abrasive wear of polypropylene/Cloisite 30B/Elvaloy AC 3427 nanocomposites. J Compos Mater 52:1833–1843. https://doi.org/10.1177/0021998317734624
21. Jain S, Parashar V (2021) Critical review on the impact of EDM process on biomedical materials. Mater Manuf Process 36:1701–1724. https://doi.org/10.1080/10426914.2021.1942907
22. Meena VK, Azad MS (2012) Grey Relational Analysis of Micro-EDM Machining of Ti-6Al-4V Alloy. Mater Manuf Process 27:973–977. https://doi.org/10.1080/10426914.2011.610080
23. Dwivedi AP, Choudhury SK (2016) Effect of Tool Rotation on MRR, TWR, and Surface Integrity of AISI-D3 Steel using the Rotary EDM Process. Mater Manuf Process 31:1844–1852. https://doi.org/10.1080/10426914.2016.1140198
24. Kumar PM, Sivakumar K, Jayakumar N (2018) Multiobjective optimization and analysis of copper–titanium diboride electrode in EDM of monel 400™ alloy. Mater Manuf Process 33:1429–1437. https://doi.org/10.1080/10426914.2017.1415439
25. Vinoth Kumar S, Pradeep Kumar M (2015) Machining process parameter and surface integrity in conventional EDM and cryogenic EDM of Al-SiCp MMC. J Manuf Process 20:70–78. https://doi.org/10.1016/j.jmapro.2015.07.007
26. VinothKumar S, PradeepKumar M (2017) Experimental Investigation and Optimization of Machining Process Parameters in AISI D2 Steel Under Conventional EDM and Cryogenically Cooled EDM Process. Trans Indian Inst Met 70:2293–2301. https://doi.org/10.1007/s12666-017-1092-z
27. James Dhilip JD, Jeevan J, Arulkirubakaran D, Ramesh M (2020) Investigation and optimization of parameters for hard turning of OHNS steel. Mater Manuf Process 35:1113–1119. https://doi.org/10.1080/10426914.2020.1765254
28. Stanojković J, Radovanović M (2017) Selection of drill for drilling with high pressure coolant using entropy and copras MCDM method. UPB Sci Bull Ser D Mech Eng 79:199–204
29. Varatharajulu M, Duraiselvam M, Kumar MB, Jayaprakash G, Baskar N (2021) Multi criteria decision making through TOPSIS and COPRAS on drilling parameters of magnesium AZ91. J Magnes Alloy. https://doi.org/https://doi.org/10.1016/j.jma.2021.05.006
30. Keshavarz Ghorabaee M, Amiri M, Salehi Sadaghiani J, Hassani Goodarzi G (2014) Multiple criteria group decision-making for supplier selection based on COPRAS method with interval type-2 fuzzy sets. Int J Adv Manuf Technol 75:1115–1130. https://doi.org/10.1007/s00170-014-6142-7
31. Mishra AR, Rani P, Pandey K, Mardani A, Streimikis J, Streimikiene D, Alrasheedi M (2020) Novel multi-criteria intuitionistic fuzzy SWARA-COPRAS approach for sustainability evaluation of the bioenergy production process. Sustain 12. https://doi.org/10.3390/su12104155

32. Zagorskas J, Burinskienė M, Zavadskas E, Turskis Z (2007) Urbanistic assessment of city compactness on the basis of GIS applying the COPRAS method. 53:55–63
33. Zavadskas EK, Kaklauskas A, Turskis Z, Tamošaitiene J (2008) Selection of the effective dwelling house walls by applying attributes values determined at intervals. J Civ Eng Manag 14:85–93. https://doi.org/10.3846/1392-3730.2008.14.3
34. Srinivasan D, Ganesh N, Daniel James J, Ramakrishnan DH, Balasundaram R, Sanjeevi R, Karthik Pandiyan GSKG, MC (2022) Investigation of surface roughness and material removal rate of WEDM of SS304 using ANOVA and regression models. Surf Topogr Metrol Prop 10:25014. https://doi.org/10.1088/2051-672x/ac6c9e
35. Kumar SV, Kumar MP (2014) Optimization of cryogenic cooled EDM process parameters using grey relational analysis. J Mech Sci Technol 28:3777–3784. https://doi.org/10.1007/s12206-014-0840-9
36. Kumar SV, Kumar MP (2015) Experimental investigation of the process parameters in cryogenic cooled electrode in EDM. J Mech Sci Technol 29:3865–3871. https://doi.org/10.1007/s12206-015-0832-4
37. Selvarajan L, Sathiya Narayanan C, Jeyapaul R, Manohar M (2016) Optimization of EDM process parameters in machining Si3N4-TiN conductive ceramic composites to improve form and orientation tolerances. Meas J Int Meas Confed 92:114–129. https://doi.org/10.1016/j.measurement.2016.05.018
38. Senthilkumar TS, Muralikannan R (2019) Enhancing the geometric tolerance of aluminium hybrid metal matrix composite using EDM process. J Brazilian Soc Mech Sci Eng 41. https://doi.org/10.1007/s40430-018-1553-2
39. Selvarajan L, Manohar M, Udhaya kumar A, Dhinakaran P (2017) Modelling and experimental investigation of process parameters in EDM of Si3N4-TiN composites using GRA-RSM. J Mech Sci Technol 31:111–122. https://doi.org/10.1007/s12206-016-1009-5
40. Cláudio C, Costa APF (2012) A contribution to the measurement of circularity and cylindricity deviations. ABCM Symp Ser Mechatronics 5:791–800

Figures

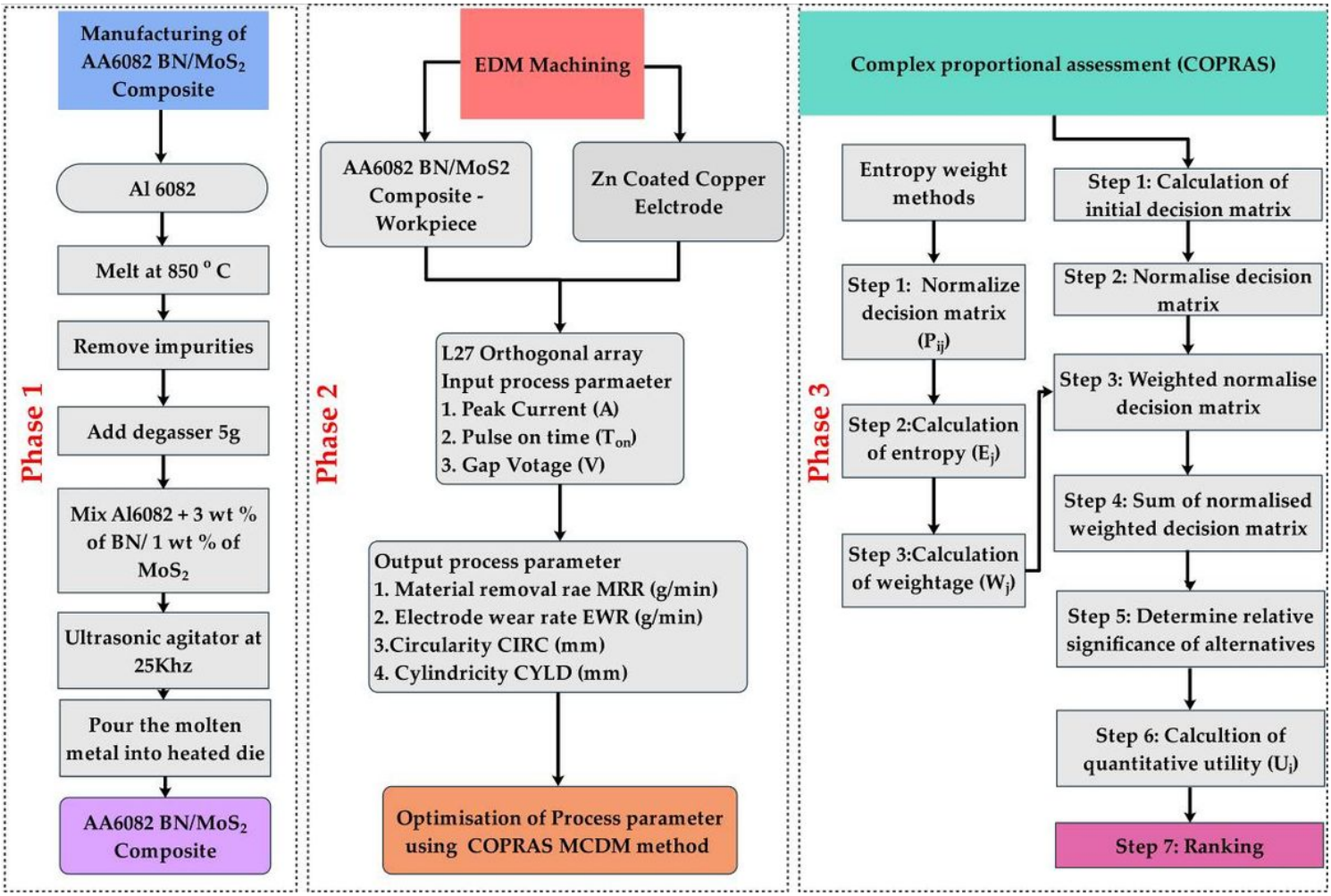

Figure 1

Schematic layout of fabrication, machining, and optimisation of hybrid composites

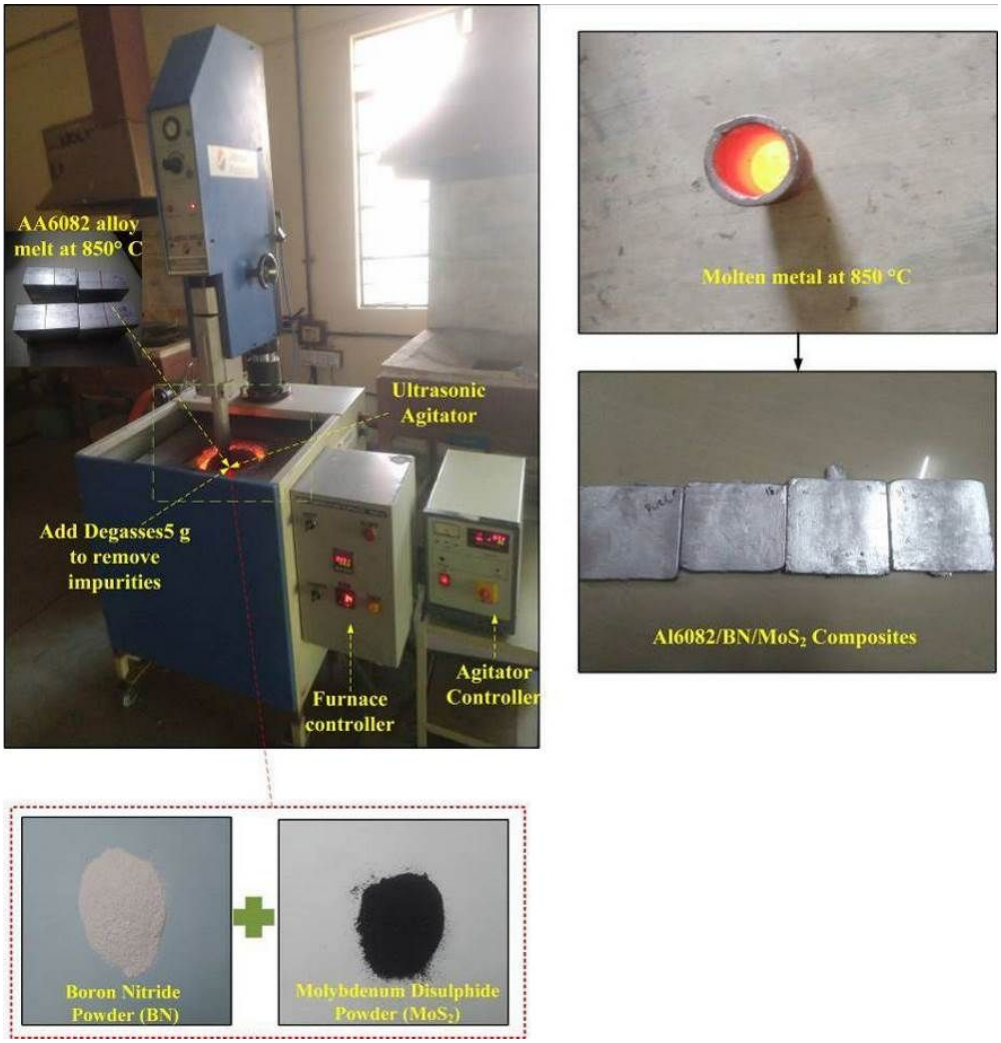

Figure 2

Schematic diagram for fabrication of AA6082 /3 Wt. % BN/1% MoS2 hybrid composite

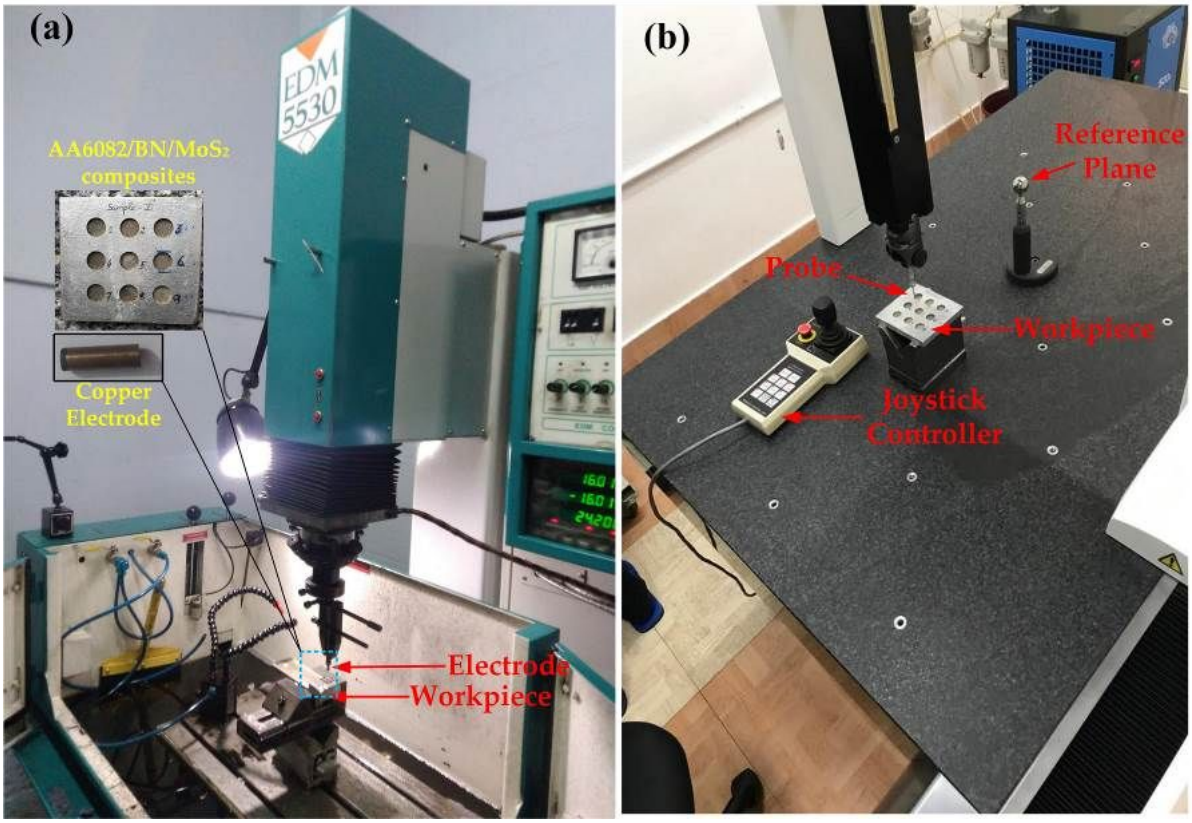

Figure 3

show the (a) Experimental setup (b) Co-ordinate measuring machine.

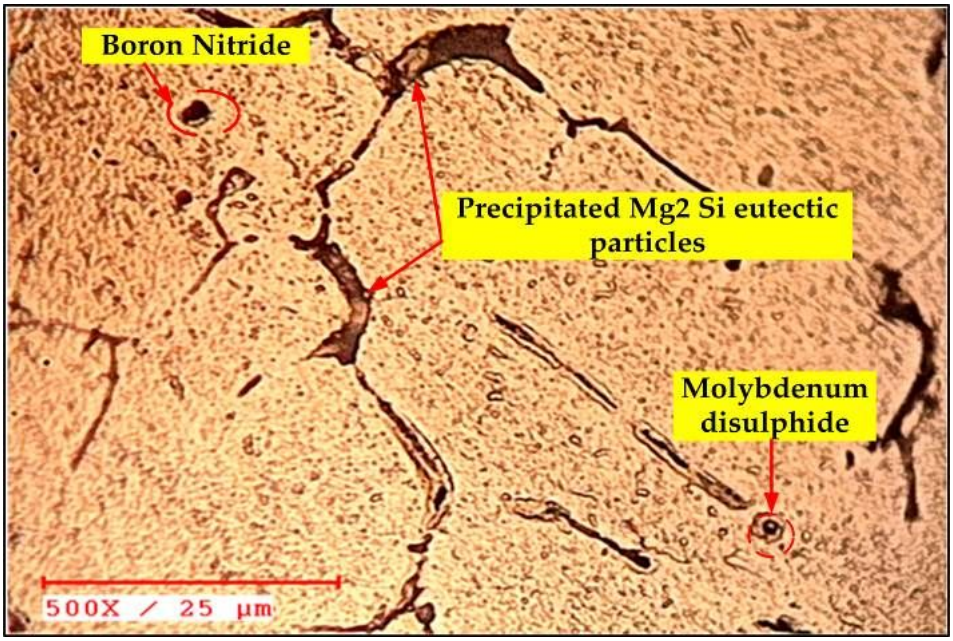

Figure 4

shows the micrographs of a matrix of stir cast AA6082 /3 Wt. % BN/1% MoS2 hybrid composite at the etched condition

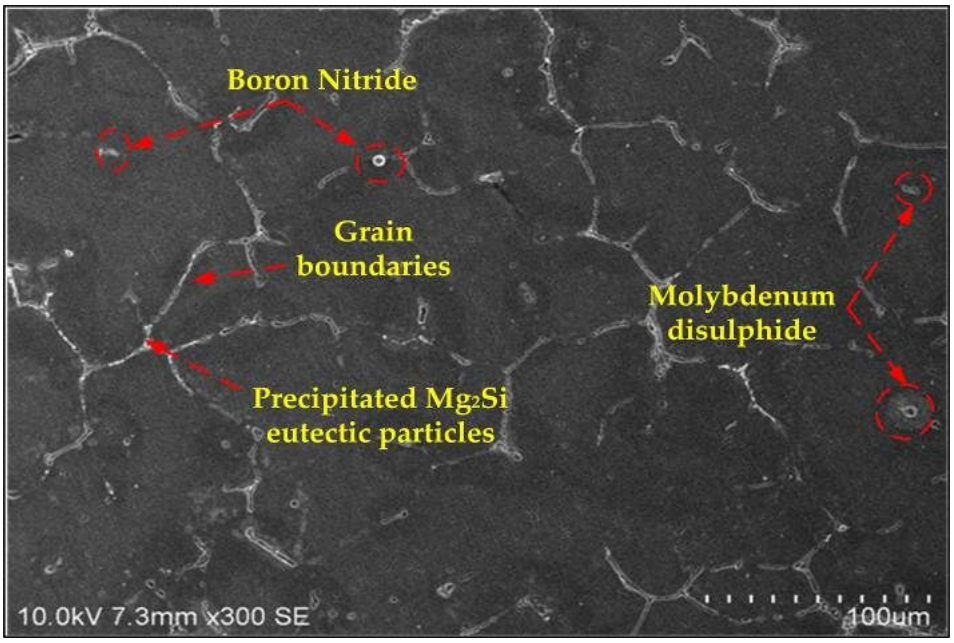

Figure 5

SEM image of AA6082/3 Wt. % BN/1% MoS_2 hybrid composite

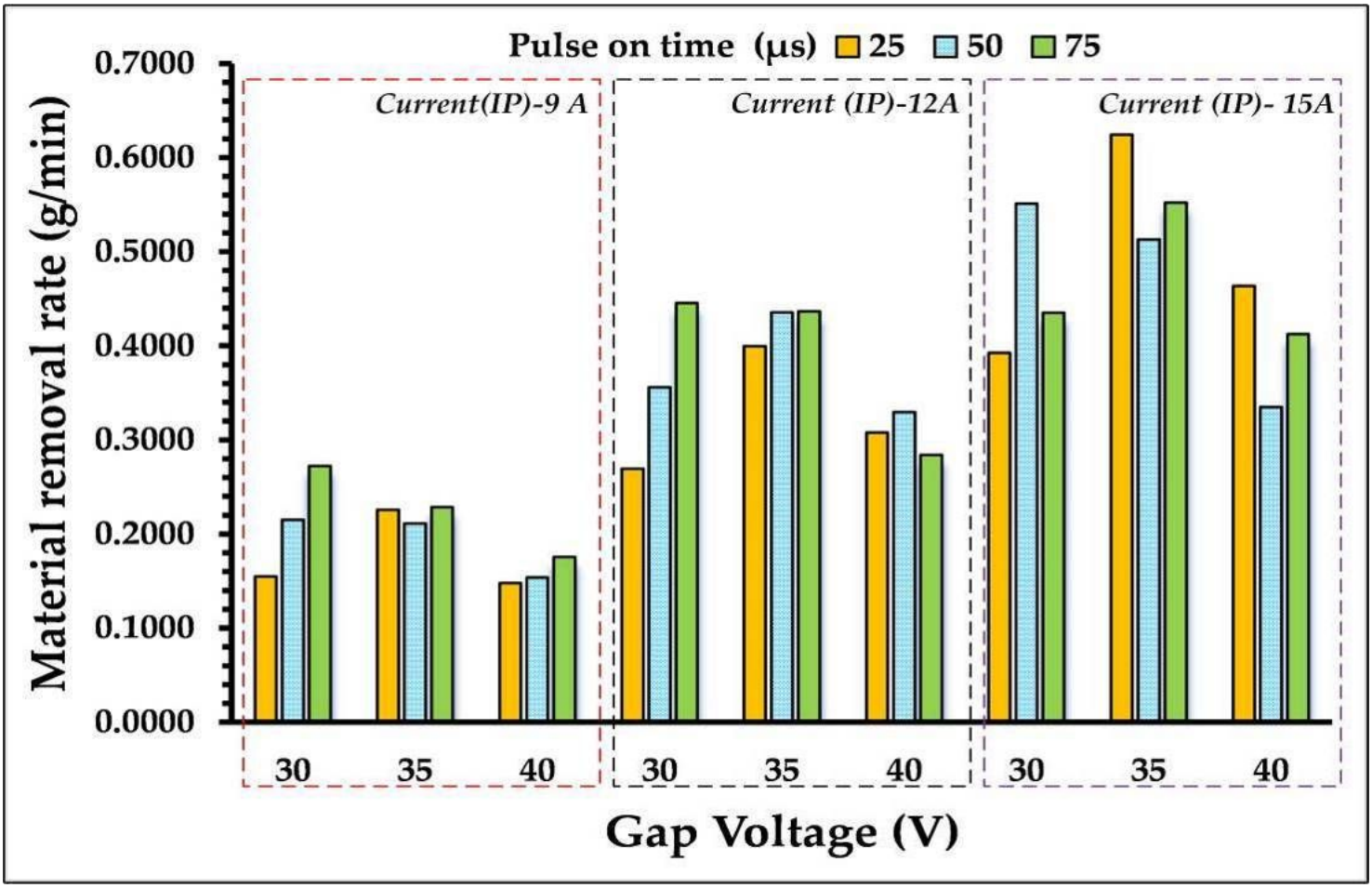

Figure 6

the Impact of input parameters on MRR.

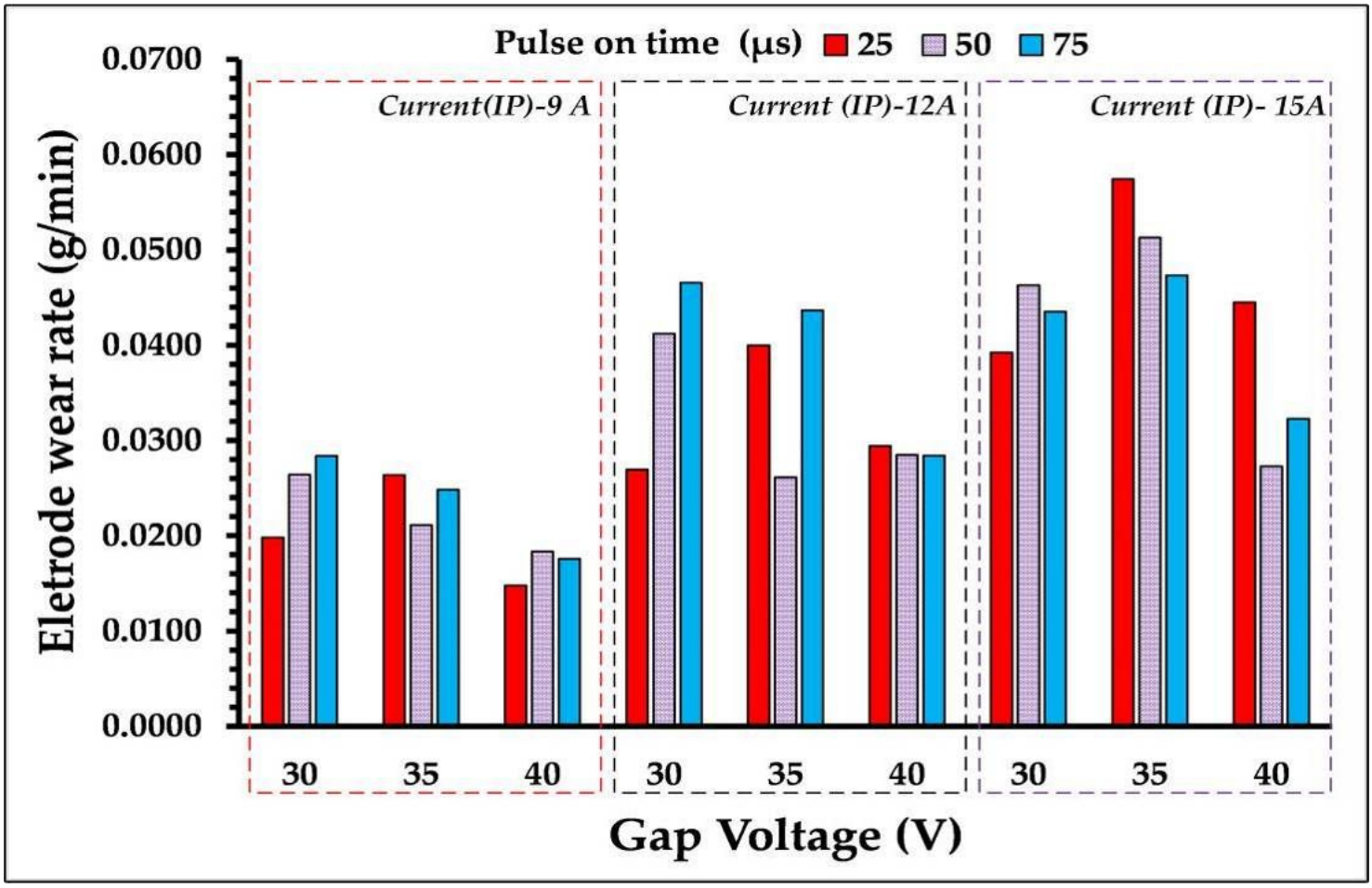

Figure 7

the Impact of input parameters on EWR.

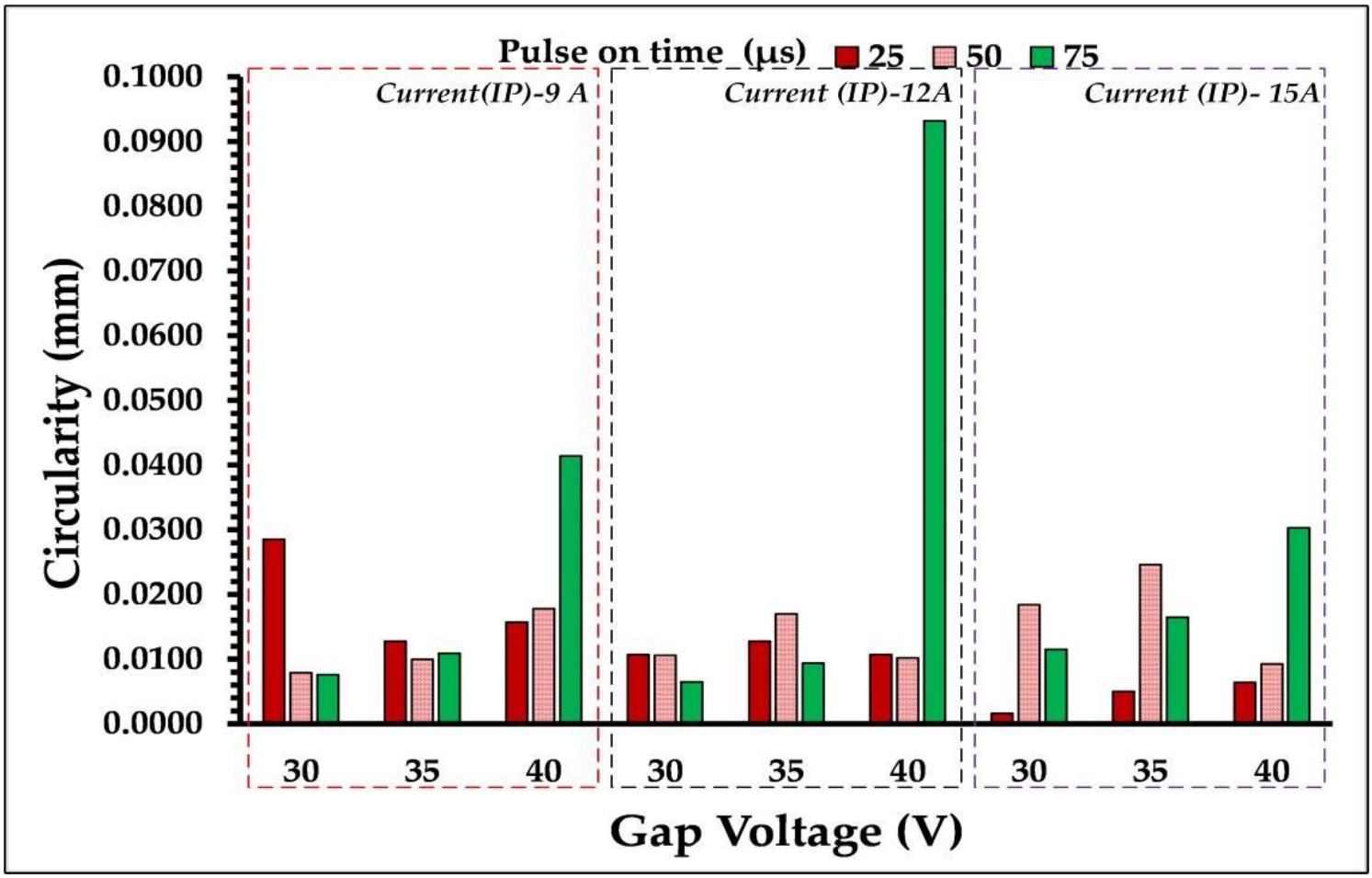

Figure 8

The Impact of input parameters on CIR.

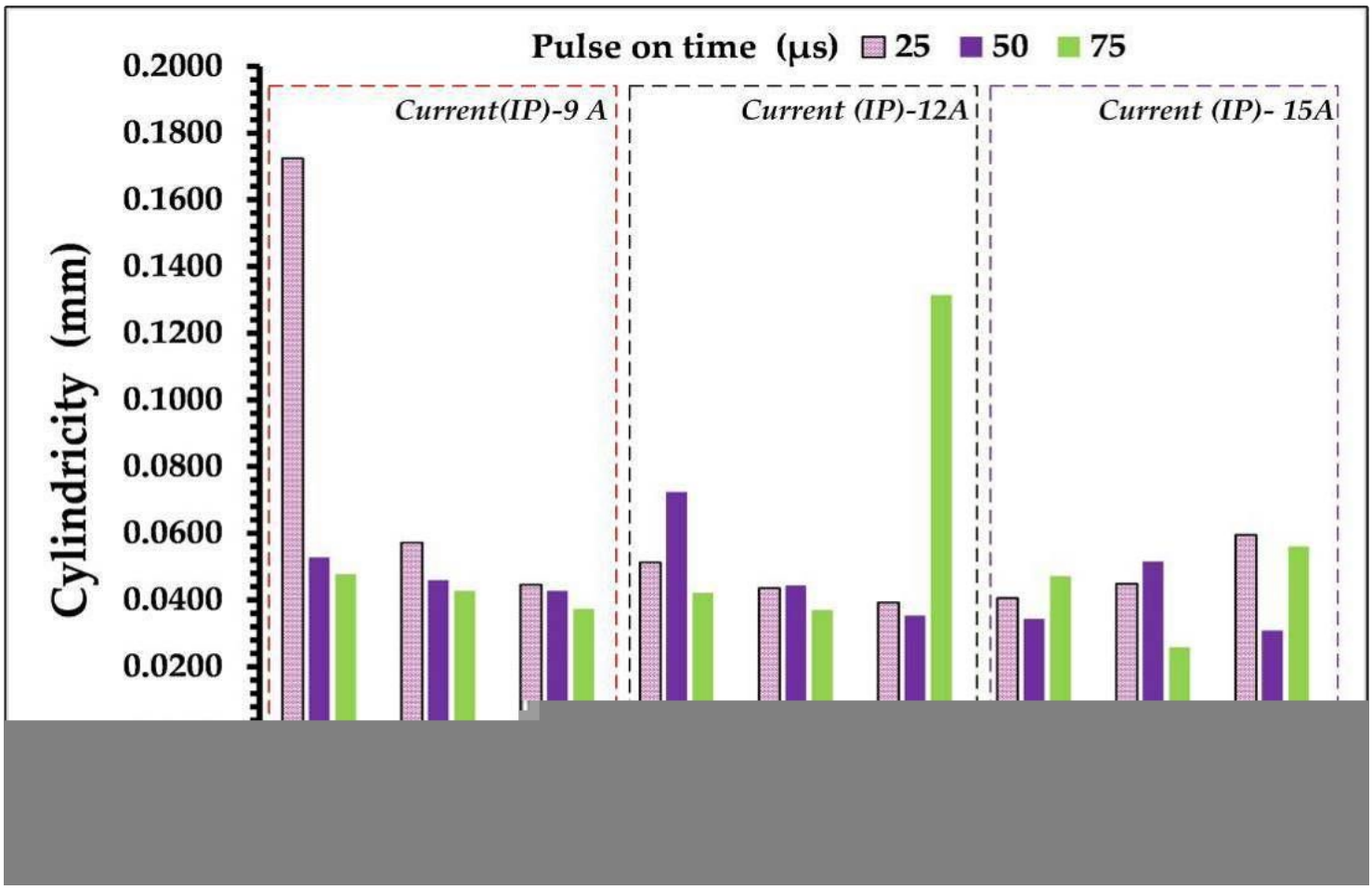

Figure 9

the Impact of input parameters on CYLD.

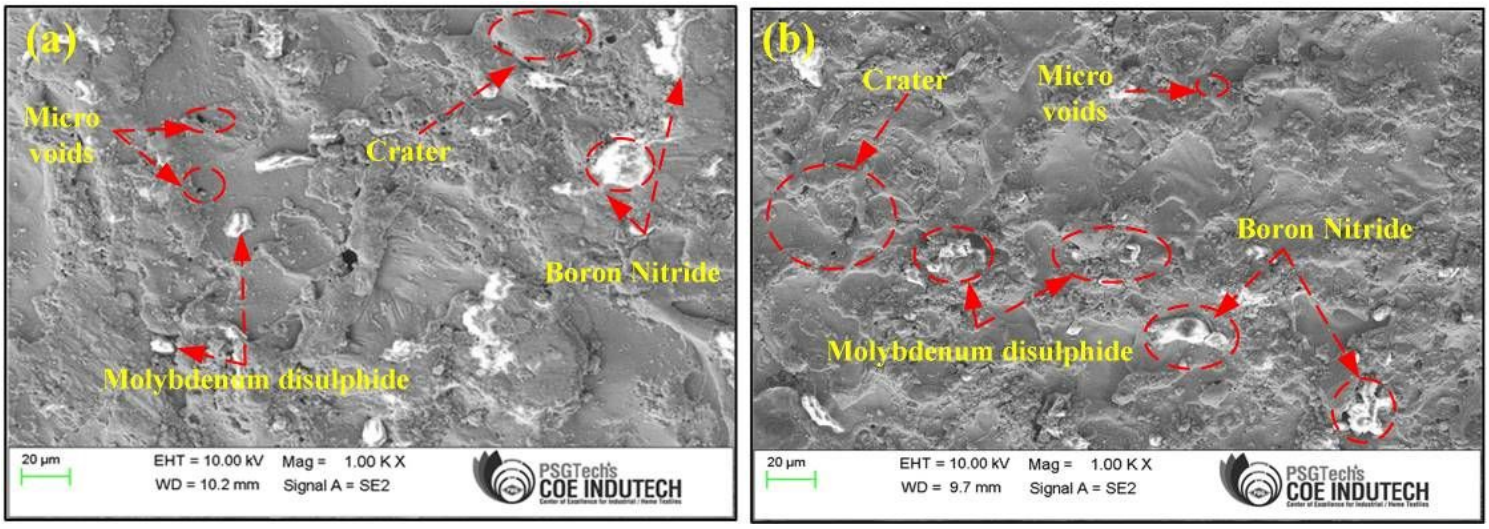

Figure 10

SEM images of EDMed surface (a) (IP) = 15A; (Ton) = 100 µs; V = 40 V. 9 (b) (IP) = 15A; (Ton) = 50 µs; V = 30 V